Anat Embryol (2001) 204:303–317

ORIGINAL ARTICLE

Z. Nadasdy · L. Zaborszky

Visualization of density relations in large-scale neural networks

Accepted: 14 June 2001

Abstract The topological organization of interfacing neuronal populations in the basal forebrain of rats was investigated in 3D by using computational methods for extracting information about the spatial distribution of cell densities and density relations. We claim that numerical and spatial constraints imposed by these methods may help to define neuronal clusters in this brain area where simple two-dimensional histology failed to reveal such an arrangement. Neuronal clusters have been suggested in many brain regions as sites of integrative operations. Taking advantage of computerized data acquisition methods in the 3D reconstruction of large cell populations we introduced four basic methods to visualize density relations on simple and combined cell markers: Differential Density 3D Scatter Plot, Iso-relational Scatter plot, Iso-density Surface Rendering and Iso-relational Surface Rendering. These methods are described and exemplified on a 3D neuronal database acquired from mapping different chemically or hodologically defined cell populations in serial sections of the rat basal forebrain.

Keywords Basal forebrain · Cholinergic neurons · Calcium-binding protein positive neurons · Cell density · Voxel · 3D visualization

Introduction

The term “basal forebrain” (BF) refers to a heterogeneous collection of structures located close to the medial and ventral surfaces of the cerebral hemispheres. This highly complex brain region has been implicated in attention, motivation, memory, cortical plasticity as well as in a number of neuropsychiatric disorders such as Alzheimer’s disease, Parkinson’s disease, and schizophrenia (Heimer et al. 1991; Dunnett et al. 1991; Everitt and Robbins 1997; Kilgard and Mersenich 1998; Sarter and Bruno 2000). BF areas, including the medial septum, ventral pallidum, diagonal band nuclei, substantia innominata and peripallidal regions contain cell types different in transmitter-content, morphology and projection pattern. Among these different neuronal populations, the cholinergic corticopetal projection neurons have received particular attention due to their demise in Alzheimer’s and related neurodegenerative diseases. However, cholinergic corticopetal cells represent only a fraction of the total cell population in these forebrain areas, which also contain various GABAergic, peptidergic and possibly glutamatergic neurons (Jones and Muhlethaler 1999; Zaborszky et al. 1999).

Figure 1 shows two composite coronal sections at different rostro-caudal levels of the BF depicting four different cell types, including choline acetyltransferase-, parvalbumin-, calretinin- and calbindin-immunoreactive neurons, which were mapped originally from adjacent sections stained for one cell marker only. When these four chemically identified neuronal populations are studied separately, each cell population shows characteristic distribution pattern. Because of the lack of adequate multiple labeling techniques and the incapacity of combining histological sections of different cell types and visualizing them in a common 3D framework, previous studies (Zaborszky et al. 1986; Jakab and Leranth 1995; Kiss et al. 1997) were focusing on the organization of BF subregions only. Due to the listed limitations these studies failed to recognize that a systematic spatial relationship might exist among these cell populations along the entire extent of the BF as suggested in a recent review (Zaborszky et al. 1999).

When multiple cell types are considered, the spatial variation of the relative density of different cell types is suggestive of the sites of integrative operations in the brain because these are the areas where neurons most

Z. Nadasdy · L. Zaborszky (✉)
Center for Molecular and Behavioral Neuroscience, Rutgers, The State University of New Jersey, 197 University Avenue, Newark, NJ 07102, USA
e-mail: zaborszk@axon.rutgers.edu
Fax: +1-973-353-1844

Present address:
Z. Nadasdy, Division of Biology, California Institute of Technology, Pasadena, CA 91125, USA

likely would share input and interact via local axonal connections. Such integrative sites are often called modules (Szentagothai 1983, Mountcastle 1998). Modules, like the columns in the cerebral cortex (Szentagothai, 1978), the striosome-matrix compartments in the striatum (Graybiel and Ragsdale 1978; Gerfen 1985), AChE patches in the superior colliculus (Chevalier and Mana 2000), clusters in the pontine (Bjaalie et al. 1991 1997) and brain stem auditory nuclei (Malmierca et al. 1998) are repetitive building blocks that may represent special sites where information processed in separate transmitter-specific streams is assumed to be integrated.

Utilizing novel computational methods, we investigated whether or not the imposition of numerical and spatial constraints may help to define hidden organizational patterns in the BF. Using computerized neuronal data acquisition methods, local density values are determined from the positions of neurons. The local density values calculated from the volume elements of the equally subdivided 3D brain construct a volumetric database that can be analyzed by a combination of numerical and visualization tools. Four such methods, 'Differential Density 3D Scatter Plot', 'Iso-density Surface Rendering', 'Iso-relational Scatter Plot' and 'Iso-relational Surface Rendering', are described here. The differential density plot and iso-density rendering are designed to reveal cluster structures in a distributed population of a single cell type. In contrast, the iso-relational visualization extracts the topological association pattern of different chemically or hodologically defined cell populations. Careful reading of the structure of cellular segregation and association allows functional hypotheses to be tested and will contribute to a better understanding of how these structural features determine information processing in normal as well as in the diseased BF.

Materials and methods

Animals and tissue processing

The reconstructions presented in this paper were prepared from data obtained from adult male Sprague-Dawley rats. All animal procedures were in compliance with National Institutes of Health Guidelines for the Care and Use of Animals in Research and approved by the Rutgers University Institutional Review Board. The anesthesia, injection of the retrograde tracers, perfusion of the animals and tissue processing has been described earlier (Zaborszky et al. 1986; Poobalasingham et al. 1996; Csordas et al. 2000). Briefly, three different types of histological material (A, B and C) were available for studying the topological organization of various cell populations in the BF:

A. In two brains (001 and 002) adjacent series of coronal sections were immunostained with antibodies against choline acetyltransferase (CH: courtesy of Dr. F. Eckenstein), parvalbumin (PV: courtesy of Dr. K.G. Baimbridge), calretinin (CR: courtesy of Dr. J.H. Rogers) and calbindin (CB: courtesy of Dr. K.G. Baimbridge) according to the ABC technique of Hsu and Soban (1981). Altogether, we obtained 48 (case 001) or 44 sections (case 002; 50 µm thick), consisting of series of sets of four sections ('layers'), stained for each marker separately. The distance between two consecutive sections stained with identical markers was 300 µm.

B. The second material consisted of 34 consecutive horizontal sections (100 µm thick) from a rat brain stained for CH.

C. The third type of material consisted of a series of coronal sections (50 µm thick) containing retrogradely labeled cholinergic and non-cholinergic neurons originating from six brains each of which received an iontophoretic injection of Fluoro-Gold (2.0% in 0.9%-saline, 8 µA DC 7 s on/off for 15 min) and a pressure application of Fast-Blue (0.3 µL 2.0% in 0.9% saline, via 30 µm tip diameter glass micropipettes) into different cortical areas. These animals survived 7 days after the surgery. In each brain, sections 400 µm apart were stained for CH.

Data acquisition

Immunostained cell bodies were digitized in BF areas with the aid of an image-combining computerized microscope (Zeiss Axioscope) system using 20 x Plan-NEOFLUAR lens and the Neurolucida software package (Glaser and Glaser 1990; MicroBrightField, Colchester, Vermont). Outlines of the sections, contours of structures and fiducial markers were drawn with a ×5 Plan-NEOFLUAR lens. Sections containing fluorescent-tagged cell bodies were mapped by using the epifluorescent setup of the Axioscope microscope equipped with appropriate filters. Fast Blue and Fluor-Gold-labeled projection neurons (exciter/barrier filter set 365/418) and the FITC-labeled cholinergic (FITC exciter/barrier filter set 450–490/520) cells could be separately visualized in the same section.

The data generated by tracing the neurons using the Neurolucida software are later referred as Neurolucida database. In the Neurolucida database, neurons were encoded by a set of records where each record consists of the x, y and z coordinates of the cell body, the section identifier, the section thickness and their number within the section. The beginning and end of a record set was encoded by a header and tail sequence, respectively. The header included the structure name and marker color for visualization. During tracing, each cell body entered with it's planar x and y coordinates relative to a reference point (e.g. the lowest midline point of the corpus callosum) common between different sections. Similarly, structure outlines were represented by their point coordinates interconnected. Sections were aligned using up to 99 alignment points for best-fit matching included in the Neurolucida software program.

In the first type of material (A), the outlines, contours and cell bodies were drawn flat by disabling z input information. Cells were plotted from adjacent series of sections alternatively stained for CH, CB, CR and PV. After plotting all cholinergic cells, areas containing such neurons were delineated using cytoarchitectonic criteria. Such borders were then superimposed on adjacent sections, stained for the other markers. Labeled cells within such defined areas were plotted. Adjacent four sections, containing markers for PV, CR, CB, and CH, were aligned using standard anatomical landmarks (i.e. corpus callosum, lateral ventricle, fornix, thalamus, optic chiasm) and collapsed into a single section (layer) by removing the within section depth coordinates but preserving the x and y coordinates of the cells, resulting in a 3D stack of 2D layers. The distance from bregma to each of this composed layer was calculated using the average of the original four sections. This way we constructed a layer set, with layers arranged according to their z coordinates and each layer containing four different cell popula-

Fig. 1 Two composite rostro-caudal (**A, B**) coronal maps to show ▶ the distribution of four cell types in the rat forebrain. Using landmarks and alignment techniques, sets of four sections alternatively stained for choline acetyltransferase (red), parvalbumin (green), calretinin (black) and calbindin (blue) neurons were compressed using the Neurolucida software so that these cells would be on a single plane. The distance between these two maps is approximately 2.4 mm (*ac* anterior commissure, *cc* corpus callosum, *CP* caudate putamen, *f* fornix, *LV* lateral ventricle, *lot* lateral olfactory tract, *sm* stria medullaris, *3* third ventricle). *Bars* 1 mm

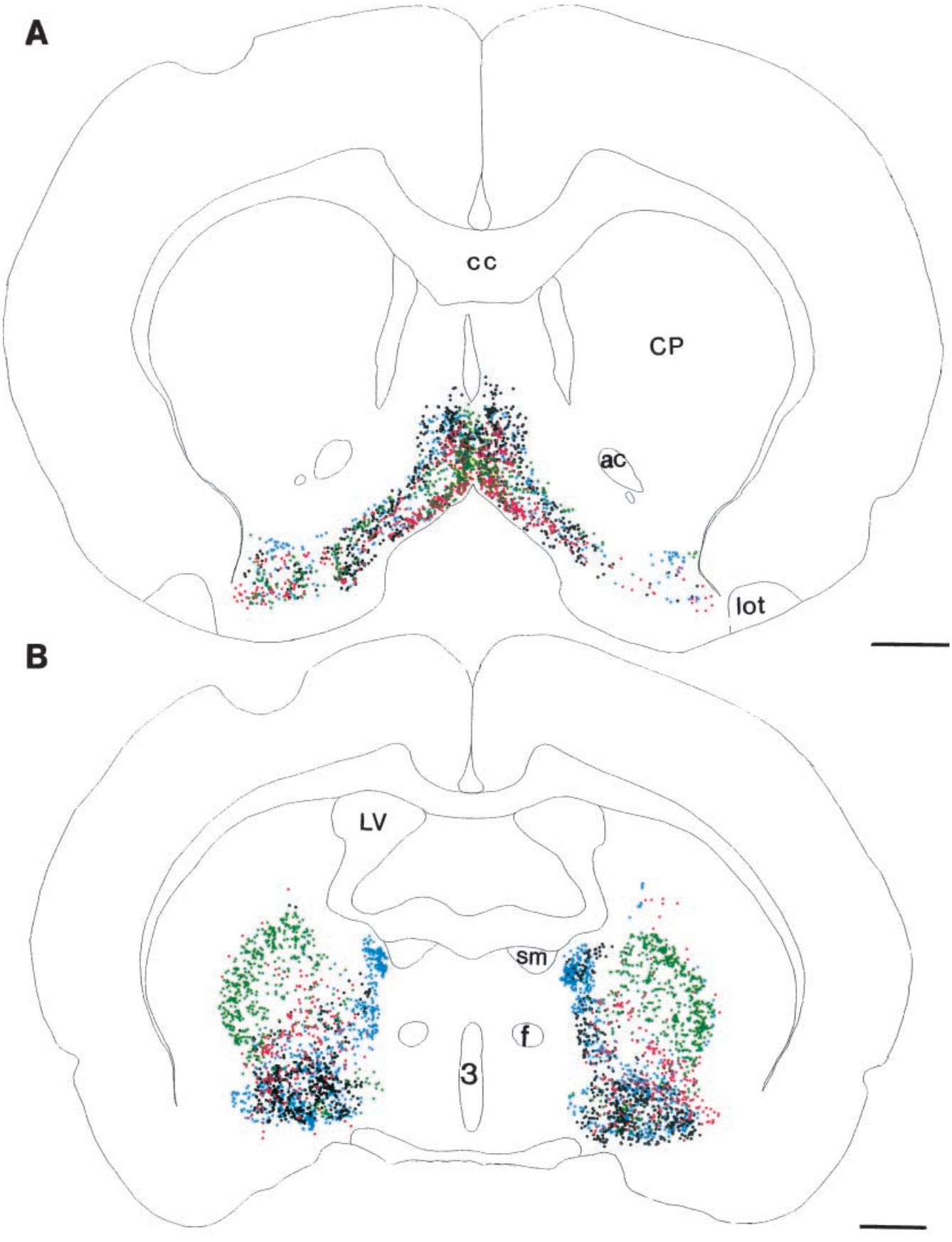
A
cc
CP
ac
lot
B
LV
sm
f
3

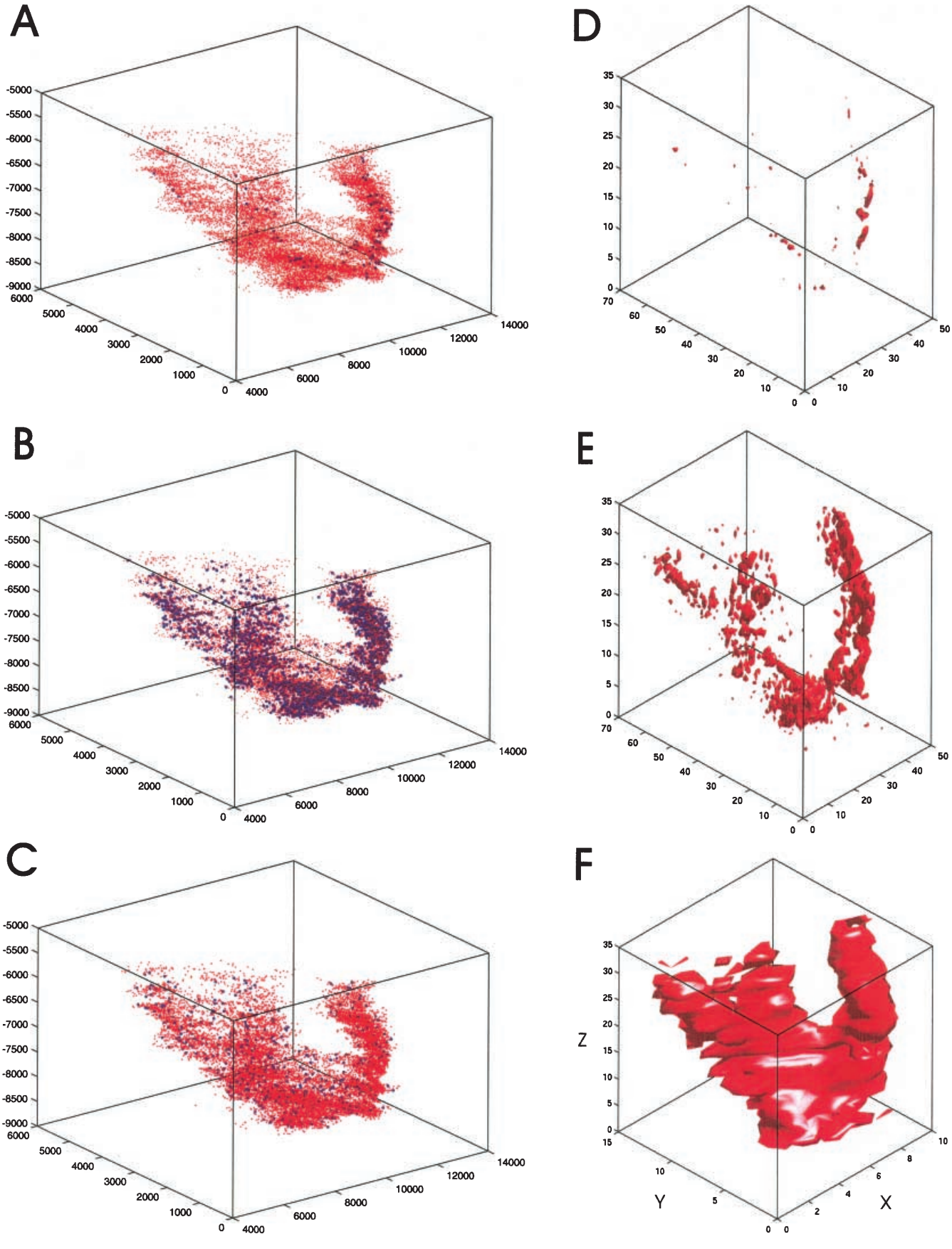
A
B
C
D
E
F
Z
Y
X

tions identified by their type and original x, y coordinates. Two of these composite layers are shown in Fig. 1. The dataset from the stack of these aligned layers served as the basis for the analysis documented in Fig. 5 from case 002. Figure 4 shows the analysis from brain 001, but the cell bodies were kept at their original z coordinates. Cells were mapped from both hemispheres in both brains, but only the right hemisphere is visualized in the renderings of Fig. 5.

The second dataset (from material B) contained a stack of aligned 34 horizontal sections, containing approximately 15,700 cholinergic cell bodies, mapped from the left side of the brain. In this brain, the z-coordinates of the cells were on-line calculated from the increment of the optical plane at which the cell body was in focus; however, section outlines and contours were drawn flat given a predetermined z-value aligned to the top of the section in the series according to the atlas of Paxinos and Watson (1998). Fig. 2 contains analyses from this material.

The third material (C) consisted of six series of brain sections (each consisting of 16 sections), each with two retrograde tracer injections. Labeled cells were mapped from every eighth section at a magnification of ×20. In this material, in order to compare data from several brains, sections were visually aligned to the corresponding map of a 'master' brain with the aid of surface contours, and fiducial markers, including the corpus callosum, anterior commisure, internal capsule, stria medullaris, stria terminalis, and the fornix. To create a maximum fit, an interactive procedure was used, including moving, rotation and shrinkage corrections along the x, y, and z-axes. For alignment and warping, we used Micro3D (Oslo Research Park, see also Brevik et al. this issue) visualization software on a Silicon Graphics Octane workstation. The renderings on Fig. 3 were derived from this dataset.

Construction of volumetric data of neuronal density

For the quantization, all Neurolucida databases were parsed for cell body and structure outline coordinates and they were compiled to ASCII files containing only the cell bodies $\{b_t\}$ of a given cell type t represented individually by the Cartesian coordinates $\{p_{xyz}\}$ and section identifier s. If z-coordinates were not available or different cell types belonging to the same layer were mapped from adjacent sections, the section identifier was taken as z-coordinate.

$$b_t = p_{xyz}\,. \tag{1}$$

Conversely, since a given position could be occupied by only one cell body, a triplet of coordinates with the cell type together completely determined cell b_t as x_b, y_b, z_b, t. Structure outlines were compiled to separate files. The medial, lateral, dorsal and ventral extremes of the entire cholinergic cell distribution were taken as the edges of a 3D framework to incorporate the entire space occupied by cholinergic cells. The total volume V occupied by neurons (neuronal space) is expressed as a vector $\vec{r}$ with minimal $\rho_{\vec{r}}$ density function.

$$V = \{\vec{r}\colon \rho_{\vec{r}} \neq 0\}. \tag{2}$$

For quantization of regional density differences, V was subdivided into identical size virtual blocks denoted as 'voxels' and defined as follows.

$$v = d_x, d_y, d_z, \tag{3}$$

where d is the edge of the voxel. The thickness of the original sections served as d_z. If different cell types were mapped from different but adjacent sections then their z_b coordinates were collapsed into a common two-dimensional plane (master plane) by removing the within-section depth coordinates, however, preserving the x and y coordinates and constructing new z-coordinates from the section identifier of cells. Thus, voxel and cell definitions have been simplified as $v_s = d_x$, d_y and $b_i = p_{xys}$, respectively. The i, j, k indices of a voxel containing a $b_i = p_{xys}$ cell body is calculated as

$$i = d_x\,(x_p / V_{length}),\ j = d_y\,(y_p / V_{width}) \text{ and } k = s. \tag{4}$$

Cells were then counted in each voxel for each cell type separately providing a local density function ρ.

$$\rho_{(v_{ijk})} = count_{(v_{ijk})} = nb_i \tag{5}$$

For visualization, we define a volume Ω based on a function of minimum density σ.

$$\Omega = \{v_{ijk} : \rho_{(v_{ijk})} \geq \sigma\}. \tag{6}$$

To investigate the anatomical distribution of high-density locations a manifold is determined that renders volume Ω with a surface and is denoted as $\delta\overline{\Omega}$. The surface rendering was carried out by using the 3D-visualization functions of Matlab software package (MathWorks, Natick, Mass.). In the visualizations we used two coordinate systems. One with coordinates of the cells as traced by the Neurolucida system. These coordinates are in micron and relate to the distance of a given point from the reference point. The plots in Figs. 2A–C and 4 use this coordinate system. The other system uses the voxel coordinates (box plots) as applied in Figs. 2D–E, 3, 5. The angles of views are independent from the axis scaling and also indicated by the Azimuth and Elevation angles given at each figures.

◀ **Fig. 2A–C** Differential density scatter plot. Red dots represent all cholinergic somas (total plotted cell number = 15,777) Blue symbols represent voxels (100×100 µm) where (**A**) the cell density is 8 or higher, (**B**) 3 or more and (**C**) cell density is 8 or more but the voxel size is 500×500 µm. Axis scaling is in µm corresponding to the x, y and z coordinates according to the Neurolucida database. Azimuth=–38, Elevation=30. **D–F** Iso-density surface rendering of cholinergic cells using the same parameters on the same dataset as in **A–C**. **D** Fragmented 3D volumes are rendered around voxels (100×100 µm) containing eight or more cells. **E** 3D volumes of cholinergic cells obtained by rendering the voxels (100×100 µm) of density ≥3. **C** Iso-surfaces of larger voxels (500×500 µm) covering density ≥8. In panels **D–F** the numbers along the z-axis represent layers (sections) and the x, y axes correspond to the voxel indices. Azimuth=-46, Elevation=34. Left part of the models (V shaped configurations in **A, C, E**) represent cholinergic cells around the globus pallidus, right part of the models (single 'column' in **A–C** or double 'columns' in **E**) belongs to the septal region of the forebrain. The z-y plane corresponds to the sagittal plane, the x-z plane to the coronal plane and the x-y plane to the horizontal

Results

In this section the methods of 'differential density 3D scatter plot', 'iso-relational scatter plot', 'iso-density surface rendering' and 'iso-relational surface rendering' are described from three aspects: rationale, algorithm and application. Biological results are presented in the application subsections. Problems of interpretation and issues common to all methods are dealt in the Discussion.

Differential density 3D scatter plot

Rationale

When plotting a population of neurons in 3D the overlapping of dense symbols makes the appreciation of true density differences difficult. One way of disambiguating cells in the cloud of overlapping symbols is to rotate the coordinate system. Concerning density differences, this method is still biased by subjectivity. An alternative

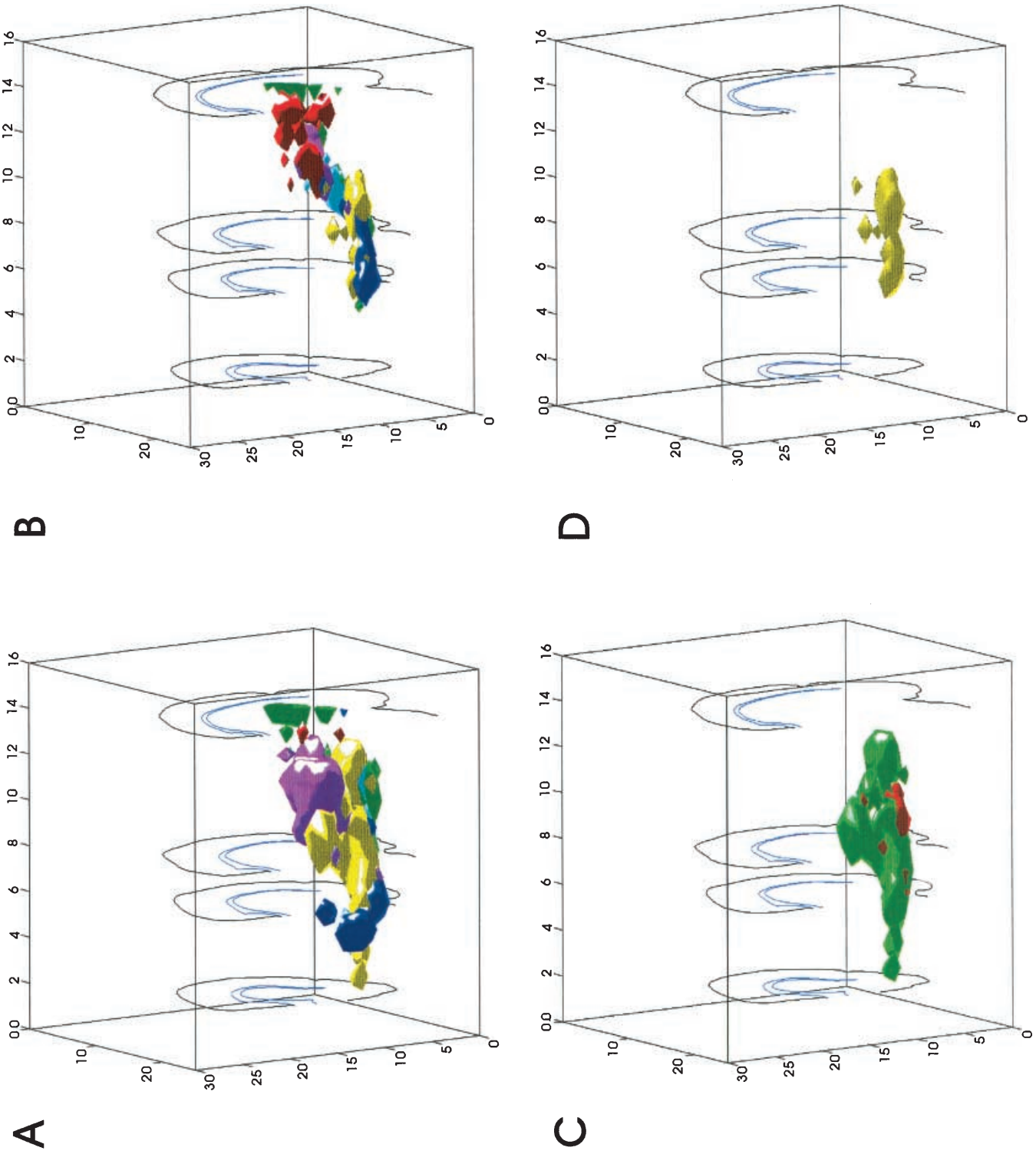

Fig. 3A–D Iso-density surface renderings to show the pattern of organization of corticopetal cells in the basal forebrain. **A, B** Retrogradely labeled non-cholinergic (**A**) and cholinergic (**B**) neurons projecting to different cortical areas are covered by different color-coded iso-surfaces. *Yellow*: medial prefrontal cortex; *red*: posterior part of the fronto-parietal cortex; *dark blue*: postero-medial (M1/M2) cortex; *magenta*: lateral frontal; *green*: posterior insular-perirhinal; *light blue*: agranular insular-lateral orbital cortices. Note that in **A** and **B** the same color code is used to represent both the cholinergic and the noncholinergic neurons that project to the same target area. **C** Location of non-cholinergic (green) and cholinergic (red) cells projecting to the medial prefrontal cortex. **D** cholinergic cells projecting to the medial prefrontal cortex. Note that the same green surface of panel **C** is rendered with yellow color in **A** and the red surface is visualized with yellow in the composite cholinergic map of **A**. Lateral view, rostral is left, caudal part of the brain is to the right. A wireframe of the outlines (black) and the corpus callosum (blue) of four sections are added to each figure for aiding orientation. The section outlines represent the right hemisphere and the view is from a mid-sagittal orientation. Azimuth=145, Elevation=10. Voxel: 400×400 µm; density ≥3. The numbers along (0–30) x and y-axes correspond to the voxel indices. Numbers 0–16 along the z axis indicate layers (sections). For further explanation, see text

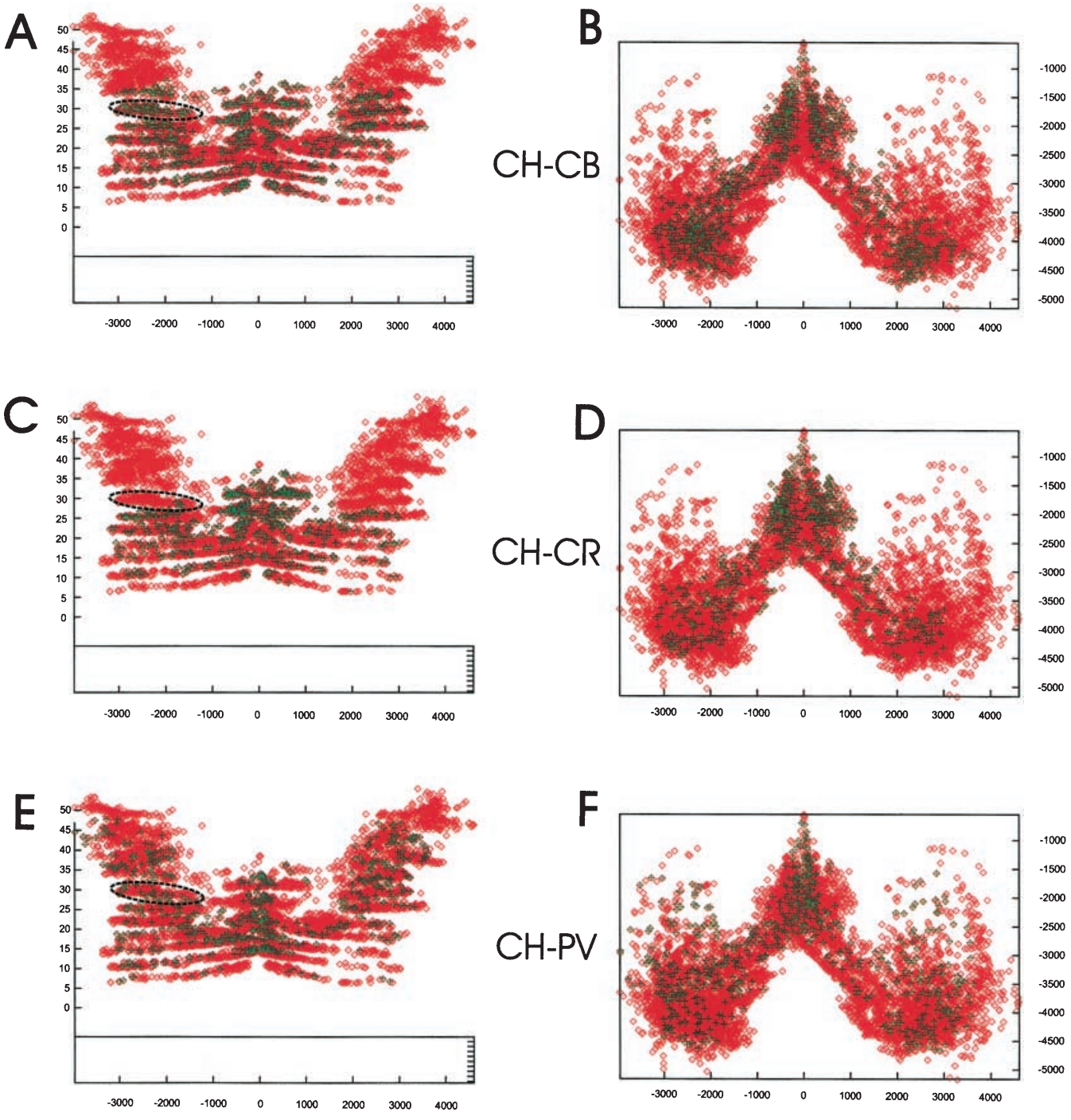

Fig. 4A, B Iso-relational scatter plot of cholinergic/calbindin neurons (CH-CB), **C, D** cholinergic/calretinin cells (CH-CR), and **E, F** cholinergic/parvalbumin (CH-PV) neuronal populations in the basal forebrain of brain 001. In these models cholinergic cells (green symbols) that fulfill the defined density threshold are overlaid on the plot of all cholinergic neurons (red symbols). Note that a group of cholinergic neurons outlined by hyphenated lines (**A, C, E**) is characterized by differential relationship to CB, CR and PV cells. Voxel: 100×100 µm, minimal ratio of cell counts is 0.25:1 between the cholinergic and all other cell types. **A, C, E** The stack of sections are viewed from above (horizontal direction); **B, D, F** antero-posterior view (coronal direction). Numbers along the y-axis in **A, C, E** represent section identifier (this material consist of 48 sections and the cell bodies are visualized in their original position), values along the y-axis in panels **B, D, F** correspond to the dorso-ventral coordinates (µm). Plus and minus values along the x-axis in both columns correspond to distances (µm) in left and right directions from the midline as determined by the Neurolucida plotting. For further explanation see text

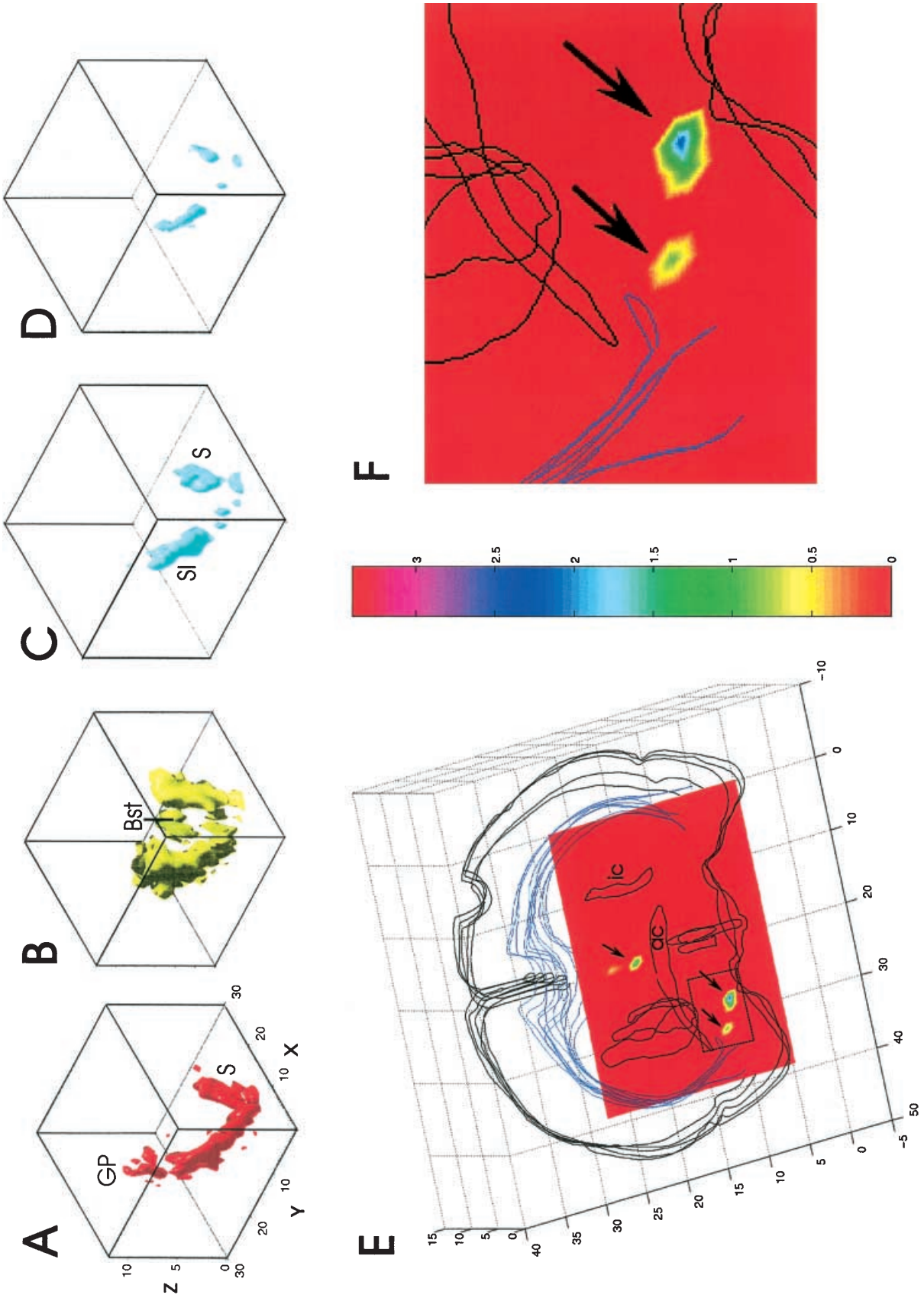
A
GP
S
z
y
x
B
Bst
C
Sl
S
D
E
ic
oc
F
3
2.5
2
1.5
1
0.5
0

method for representing true density differences is to convert the density of cells to 2D iso-density maps (Vassbo et al. 1999). The obvious limitation of this method is the lack of the third dimension. We suggest a new method that quantifies density differences first, and then plots the density markers in a 3D coordinate system. In general, this method can be applied to quantify and map the spatial distribution of any variable related to a single neuronal population. Our main interest was to visualize density differences in the cholinergic cell populations of the BF in a 3D coordinate system, primarily because this could reveal clusters in the neuron population that may correspond to cooperative elements of the network.

Algorithm

We assume that the input data is provided as point coordinates of cell bodies in the Cartesian 3D space. In the simplest data structure each row represents a single cell given by the *x*, *y* and *z*-coordinates relative to a reference point as origin (Eq. 1). The original *z*-coordinates can be substituted by the layer identification and vice versa. We further refer to this data file containing the sufficient and necessary parameters from Eq. 1 as the input data file. After the cell bodies have been defined by their point coordinates they are placed into a grid system that partitions the neuronal space into voxels (Eqs. 3, 4). Next, cells located inside a given voxel are counted (Eq. 5). Voxels with cell counts larger than a predetermined density are represented by a single marker. The precise position of the marker is given as a cell body selected randomly from the pool of neurons contained by the given voxel. The distribution of these markers highlights locations where neurons form cluster.

Application

Inspection of sections stained with the cholinergic marker choline acetyltransferase suggests that the density of cholinergic cells is not uniform. As can be seen in Fig. 1 the red symbols, representing the cholinergic cells, often form aggregates. Figure 2A–C, using differential density scatter plots, investigates whether neurons are organized in clusters or distributed homogeneously. For comparison, panels D–F in this figure displays density differences in the same dataset using iso-density surface renderings that will be described in the next paragraph. In panels A, B of Fig. 2 the total volume of this cholinergic neuronal space (4.3×7.1×3.4 mm) was partitioned into 100×100 µm voxels in the *x* and *y*-axes and 34 layers in the *z*-axis, respectively. This subdividing of the neuronal space resulted in 103,802 voxels. In comparison, panel C of Fig. 2 illustrates the same neuronal space subdivided by 500×500 µm voxels resulting in 3,808 voxels. By scanning the database of cellular densities with different thresholds, we were able to delineate sub-spaces where the highest cell density occurred. Qualitative verification of a cluster organization is possible by comparing individuals of the same species. If high-density markers occur at similar locations between individuals in spite of the independent sampling then the cellular density is unlikely to be controlled by chance. Besides the qualitative analysis, the density measure allowed us to make quantitative statements about the distribution of neurons. For example, the densest upper 20% of cholinergic neurons are located in 8% of the voxels. Our preliminary study, using a similar approach in the brain of a *Macaca mulatta*, showed that the same proportion (20%) of cholinergic cells occupies a smaller proportion of voxels in this monkey brain, suggesting that a larger percentage of neurons are aggregated into clusters in the primate BF (Zaborszky et al. 1999). Similarly, to the cholinergic cells, the other three cell populations, including calretinin, calbindin and parvalbumin-containing neurons in rat, show inhomogeneous distributions (L. Zaborszky, D.L. Buhl, S. Pobalashingham, J. Somogyi, J.G. Bjaalie, Z. Nadasdy, unpublished work).

◀ **Fig. 5A–F** **A** Iso-density surface rendering of cholinergic cells from the right side of brain 002. **B** Iso-density surfaces of calretinin cells from the same brain. Voxels (250×250 µm) containing five or more cells. **C** Iso-relational surface rendering of cholinergic and calretinin cells. The spatial relationship of cholinergic neurons to calretinin neurons was determined by mapping the change in their density ratios. The ratios between the cholinergic and calretinin cells were calculated considering only those voxels where both cell types have a density ≥ 5 cells and their minimum ratio was 0.25:1. **D** Iso-relational surfaces of cholinergic/calretinin cells are shown with the lowest local ratio: 1:1. In these models areas closer to the left of the coordinate system represent caudal (*GP* globus pallidus), those parts that are closer to the right belong to more rostral (*S* septal) region of the basal forebrain (*Bst* bed nucleus of the stria terminalis). Numbers along the z-axis indicate the composite layers (sections), numbers along the x and y-axes correspond to the voxel indices. Azimuth=–46, Elevation=34. **E** Splicing the volumetric data and projecting the density data onto a coronal plane. This map represents the change of relative density of cholinergic and parvalbumin cells as collapsed into the coronal master sections. Different relative densities are color-coded. The highest density ratio between cholinergic and parvalbumin cells (≥2:1) is indicated by blue, the lowest (≥1:4) is indicated by red and the 1:1 ratio is indicated by green. In order to provide anatomical localization, the maps were inserted to the 3D wireframe of anatomical structures traced from the original sections. The z-axis in this plot is the one with numbers from 0–15 indicating the layers (sections). Numbers along the y-axis (-5-[40]) and the x axis (50-[-10]) correspond to the voxel indices. In order to give a 3D view, the brain is slightly tilted to the left and towards the viewer. Azimuth=–104, Elevation:=78. Note the clusters of cells in the septum (*one arrow*) and in the horizontal limb of the diagonal band (*two arrows*). Splicing the volumetric data layer-by-layer revealed no hollow spaces inside the iso-relational surfaces. **F** Enlarged view of the boxed area in panel **E** (*ac* anterior commissure, *ic* internal capsule)

Iso-density surface rendering

Rationale

Spatial distribution of different cell types may be very complicated as neuronal populations interdigitate, inter-

sect, or overlap with one another. Instead of using scatter plots, with which the comparison of more than two cell types becomes increasingly difficult, the spatial organization of density differences is better visualized by rendering a surface around cell groups with identical density. The 'iso-density surface rendering' is similar to the 'differential-density 3D scatter plot' in the sense that a selected subset of voxels is visualized. However, instead of representing them by single points the algorithm renders a surface around voxels larger than a selected cellular density. The advantage of this method is that multiple cell types can be compared using the same density threshold and voxel size.

Algorithm

The procedure of subdividing the 3D database into voxels and calculating the voxel cell densities is identical to that of the 'differential-density scatter plot'. Conversion of the Cartesian 3D point coordinates of the somata to local density values constructs a volumetric data (Eq. 5). In contrast to the parametric database where cell bodies are represented by their x,y,z-coordinates, the entries of the volumetric database are cell counts. More precisely, the volumetric database is described by an array of 2D matrices where density values are organized in *i* rows and *j* columns according to the coordinates of corresponding voxels given by Eq. 4. Each 2D matrix represents a brain section. For visualization of the cell density distribution, a density threshold is defined and voxels larger than the threshold are identified (Eq. 6). For surface rendering, different software packages use different realizations but the algorithm is essentially the same. Briefly, the generic algorithm first renders a 3D skeleton on the selected and smoothed voxels. Then it determines a 2D manifold on the skeleton by interconnecting points that separate the higher density space from the lower density space. The manifold is further partitioned into triangles and triangles are rendered by surface elements with specific surface properties. These surface elements are then smoothed by cubic spline interpolation and reflectance properties as well as a light source are defined.

Application

To familiarize with the essential features of the iso-density surface mappings, Fig. 2D–F demonstrate density differences in the same dataset as of Fig. 2A–C, however, instead of the scatter plot method, surfaces are rendered around cell groups with similar densities. To resolve large-scale inhomogeneities, in Fig. 2F the size of the voxel was chosen to be 500×500 μm and voxels containing eight or more cells were 'covered'. Comparing this plot with the map of Fig. 2C suggests that the surface rendering in Fig. 2F captures the gross features of the cholinergic system, however, regions with few cholinergic cells cannot be separated from high cell density locations. The algorithm in Fig. 2E rendered a surface around voxels of 100×100 μm with 3 or more cells per voxel. By eliminating regions with very few cholinergic cells, this rendering seems to incorporate both the general shape of the entire cholinergic continuum as well as some of the local density differences. Note that the rendering in panel E used the same thresholding and voxel size as the scatter plot analysis of Fig. 2B with comparable results: featuring the skeleton of the cholinergic system, including the V shaped distribution of cells around the globus pallidus. Finally, in the plot of Fig. 2D, using the same voxel dimensions and density threshold as in Fig. 2A, the familiar shape of the cholinergic system is hardly appreciable. These series of plots demonstrate that to avoid misinterpreting topological relationships among multiple cell populations (see below), using iso-surface renderings the proper spatial and numerical features of the individual cell populations need to be first established.

Cholinergic cells in rodents as well as in primates project to different cortical areas according to a rough medio-lateral and antero-posterior topography (for references see: Woolf 1991; Wainer et al. 1993; Mesulam 1996; Zaborszky et al. 1999). It is unclear, however, to what extent cell populations projecting to functionally distinct cortical areas are separated or overlapped in the BF. Since various inputs to the BF show regional localization, it would be important to know whether or not functionally distinct cortical areas can be independently modulated via the BF. Since a scatter-plot representation or the overlap analysis as routinely applied (He et al. 1993; Alloway et al. 1999; Leergaard et al. 2000) allow the simultaneous comparison of only two cell populations, in order to appreciate the overall projection pattern, Figs. 3A, B display a composite of the iso-density maps of non-cholinergic and cholinergic cell populations that project to six different cortical targets as indicated by different colors. These renderings suggest, that the high density locations of these non-cholinergic (Fig. 3A) and cholinergic (Fig. 3B) populations are separated in the BF. Since individual cells are replaced by densities and densities are rendered around by surfaces, the simultaneous 3D visualization of multiple cell populations is feasible. In these renderings, we used a 400×400 μm voxel grid and a density threshold ≥3 per voxel. From the composite maps, panel C in Fig. 3 shows the rendering of a subpopulation of non-cholinergic (green) and cholinergic (red) cells that project to the medial prefrontal cortex. Comparing the plots of panel C with the separate plot on Fig. 3D illustrates that the cholinergic cell group (red in C and yellow in D) is surrounded and partially covered by the larger surface (green) of the non-cholinergic cell group. Therefore, to appreciate the real dimension of individual cell types the composite representations must be compared with individual representations. The flexibility of combining and decomposing cell groups of different types is a critical feature of the method.

Iso-relational scatter plot

Rationale

In order to understand whether information is transferred in 'private' (segregated) or via 'shared' (overlapping) channels it is important to investigate the spatial relation of interfacing neuronal populations in the brain. The reconstruction of spatial relations from a two dimensional image of cell populations plotted in a 3D coordinate system is ambiguous. A 3D scatter plot may characterize many qualitative aspects of the spatial distribution of a single cell type; however, it is very difficulty to resolve spatial relations of different cell types. Two cell types may group together either because they are located close together in the Cartesian coordinates or because they overlap when observed from a certain point of view. Visually, it is impossible to separate sub-spaces occupied by a single cell type from spaces occupied by both cell types based on a single aspect. Even rotation of the coordinate system is insufficient to gain relational information when thousands of cells are considered. In order to reduce complexity and extract the associative relationship of different cell types, we calculate the density ratio of the two cell types in each voxel. Highlighting the locations at which the density ratio exceeds a certain level reveals the spatial configuration of cell-to-cell associations between different cell types.

Algorithm

The first step in subdividing the 3D coordinate system into voxels is identical to the method of 'differential density 3D scatter plot', however, it must be done for both cell types. For this, the two cell types must carefully be mapped in a common 3D coordinate system. If the different cell types were traced from different sections, it must be considered that inference of the joint density from separated sections may be artifactual. If density changes between adjacent sections are negligible, the within-section z-coordinates of different cell types can be collapsed into the same section to obtain an estimate for the real joint-density. The next step is to calculate local density ratios between the two cell types for each voxel. By assigning density ratios to each voxel a volumetric database, represented as a stack of 2D density vectors, is obtained. Scanning the database by a predefined density ratio criterion makes it possible to select voxels where a certain numerical association between cell types has been established. These spatial locations, where density ratios define associative relationships, are visualized by the random selection of a cell from the corresponding voxel and plotting all selected cells in a 3D coordinate system. This relational analysis is extendable to more than two cell types and to any specific compositions as long as the composition can be expressed as a function of local counts of different cell types.

Application

Figure 4 represents the iso-relational distribution of cholinergic/calbindin (CH-CB), cholinergic/calretinin (CH-CR), and cholinergic/parvalbumin (CH-PV) cells of the rat BF. We used 100×100 μm grid size for partitioning the database into voxels. The *z*-dimension was identical to the section thickness. As described in Materials and methods, this particular material consisted of 12 sets of layers, each layer was a composite of four sections stained for the individual cell marker that were collapsed into the same virtual plane and density ratios were calculated from the planar projection of these cells. The density ratio of our choice was minimum 0.25:1 between the cholinergic and any other cell type. This means, for example, that for a voxel to be marked it must have contained maximum four times as many calbindin as cholinergic cells in the same voxel. Those of the cholinergic cells at which this density ratio has been established are highlighted by green symbols and overlaid on the scatter plot of all cholinergic neurons. Groups of cholinergic neurons are easy to distinguish from other cholinergic cells based on their specific numerical and spatial relationship to the other cell types. For example, on the dorsal view of the models a cholinergic cell group is outlined (panel A) on the left side of the brain where the density of both cholinergic and calbindin cells met two criteria: (1) the number is at least five for each cell type within the voxel and (2) the minimum ratio of cholinergic to calbindin cell counts is 0.25. However, in the same general region, considering the cholinergic-calretinin iso-relational scatter plot (C), there are almost no green symbols, indicating that no similar relationship exists in this location between cholinergic and calretinin cells. Finally, in the same region, different subgroups of cholinergic cells are marked based upon their relationship to parvalbumin cells (E). Additional studies, using specific tracers, electrophysiological, pharmacological or genetic manipulations, should be conducted to verify that the regional segregation of such cholinergic-calbinding cell groups represents functional association of the constituent cell types.

Iso-relational surface rendering

Rationale

Initial studies with the iso-relational scatter plot method such as shown in Fig. 4 have suggested that numerical relations between cholinergic and the other three cell types are very complex and may have a regional variation. Therefore, rendering a surface around the two cell populations where a certain density ratio is detected may help to recognize better the pattern of these complex relations than by using the 'iso-relational scatter plot'. Similar to the 'iso-relational 3D scatter plot', the aim of this representation is to show the co-distributive association between two different cell types. Since different cell

types have a typically complicated spatial association, marking the associative nodes in a scatter plot does not necessarily elucidate the true 3D configuration. When relations are represented by point-like markers the spatial relations between points, such as which point is closer and which point is further from the viewer, are difficult to resolve. One way to disambiguate spatial relations of point-like markers is to rotate the database. For a stationary presentation, a better representation is to render a surface around joint voxels, where a certain density ratio of two cell types is established. This surface separates cells where a certain density ratio is higher than a critical value from cells where the density ratio is lower. Besides, the qualitative information provided by the spatial distribution, quantitative aspects of density relations are available. The unique feature of the 'iso-relational surface rendering' method is the visual representation of the abstract relationship of different cell types, that is a more relevant feature of the functioning network than the exact locations of cell bodies.

Algorithm

The first few steps are identical to the 'iso-relational scatter plot' method. The neuronal space is subdivided into voxels for both cell types. Next, the cell density ratio is calculated within each voxel that is shared between two cell types. The total volume of density ratios is compiled to a volumetric database $\rho_{(v_{ijk})}$ where density values are assigned to individual voxels (Eq. 5). This data is prepared in a format of 2D matrices where each k brain section is represented by a matrix of $\rho_{(v_{ij})}$ density values organized according to their i,j indices as rows and columns. Iso-density demarcation lines are calculated and rendered by a surface (Eq. 6). Density ratios smaller than a critical value are located outside of the surface. For visualization purpose, a range of critical density values must be applied for testing the integrity of clouds and uncovering eventual hollow spaces. The algorithm of surface rendering is the same as described at the 'iso-density surface rendering'. Complex relationships between multiple components such as density relations of multiple cell types can be decomposed into pairwise relations and visualized as merged surfaces. Color-coding of surfaces for different cell types helps to interpret complicated configurations.

Application

Figure 5A and B displays the iso-density surface maps separately for cholinergic and calretinin neurons, respectively at a density threshold of five cells per voxel (250×250 μm). The associations of these two cell types are illustrated in panels C and D using two different density ratios. In Fig. 5C the blue regions represent overlapping regions where the cholinergic/calretinin density ratio was at least 0.25:1. In Fig. 5D cholinergic/calretinin density ratios 1:1 or higher were rendered with a blue surface. In the plot of Fig. 5C, the program scanned the database for the presence of voxels where both the cholinergic and calretinin cell number were at least 5 per voxel and the ratio of cholinergic to calretinin cell counts is minimum 0.25:1. The smaller volume of Fig. 5D contains only those voxels where the minimal density of both cells types is 5 but their ratio is at least 1:1. In other words, this rendering did not contain those voxels where the cholinergic/calretinin ratio was between 0.25:1 and 1:1. Using the 'iso-relational surface rendering' technique, regions with high density of calretinin cells that contained only a few cholinergic cells were eliminated from visualizations. Comparing, for example, Fig. 5B with Fig. 5C, one can realize that the large yellow cell cluster in the middle of the model, representing the bed nucleus of the stria terminalis (Bst), disappeared in panel C; thus the spatial and numerical relationships of the cholinergic neurons to the calretinin cell population is easier to appreciate. The plot also suggests two main groups of association; one in the substantia innominata (SI) and the other in the septum (S), respectively, with a smaller group of connecting areas between them. The major advantage of the 'iso-relational surface rendering' of Figs. 5C, D, as compared to the 'iso-relational scatter plot' of the same two cell populations (Fig. 4C,D), lies in the reduction of complexity of the spatial relationships between co-distributed cell populations.

Discussion

We introduced four new methods of combining quantitative analysis with visual representation of neuronal populations in 3D space. The purpose of these methods was to provide a global view of complex data that captures the main density structure as well as the association pattern of different cell types. These two features are relevant for suggesting anatomical locations of functional segregation and integration between specific cell groups. Although our description is focused on the visualization of the data, these methods allow us to evaluate further quantitative aspects that are beyond the scope of this paper. Since the core of the visualization is the extraction of quantitative features, adding new features such as the dendritic arborization (Zaborszky et al. 2001) can flexibly be combined. To establish whether clustered association or segregation between two cell populations in a 3D space deviate from a random co-distribution, simulations by generating surrogate data on the basis of different association statistics are necessary to perform (Bjaalie et al. 1991; L. Zaborszky, D.L.Buhl, S. Pobalashingham, J. Somogyi, J.G Bjaalie, Z. Nadasdy, unpublished work).

Thresholding, cell clusters

The number of cells per voxel is influenced by the size of voxel and cell count threshold criteria. When small voxels and high cell count thresholds are used, the num-

ber of voxels selected for visualization may not be sufficient, while large voxels and low thresholds will not capture local density differences. In order to determine the optimal density threshold for detecting cell clusters, we applied different density thresholds as an independent variable. If the distribution of cell bodies is random then increasing the density threshold should monotonically decrease the number of clusters. Indeed, using lower threshold (e.g. d≥3, 100×100 µm voxels in Fig. 2B), the even distribution of blue markers suggest a random scattering of cells. In contrast, the location of clusters using higher density threshold (e.g. Fig. 2A) may corresponds to predetermined zones where the other cell populations are 'attached' to the cholinergic neurons to form mixed clusters or larger amalgamations such as seen in Fig. 5C and D. Moreover, using the density as a dependent variable, we were looking for the smallest unit volume within which local density differences can be resolved and major structural features be preserved. The optimal size was determined by employing several different grids from 50 to 500 µm. The choice of size that provided sufficient spatial resolution and resulted in the maximal number of non-empty voxels was generally at grid edges between 250–400 µm.

Problems of interpretation

Scatter plot

Differential density scatter plot and *iso-relational scatter plot representation* are both effective in locating clusters within an individual as well as in combined cell populations, respectively. In addition, they allow to compare clusters between individual brains and quantifying the dependency of the number of clusters from different density criteria and voxel sizes. They do not, however, indicate the significance of cluster structures in terms of deviation from random distribution.

Both types of scatter plots share the problem derived from the sectional separation of the 3D database. If cell markers have been traced from sections with gaps between them then the distribution of cells in the *z* dimension is discontinuous. One way to eliminate the discontinuity of data is to collapse the within-section *z* coordinates to the z coordinate of the given section. In the visualization this would show up as a multi-layer distribution. Using this transformation, we lose information about the real *z* coordinate of cell bodies but the x and y coordinates together with the section ID reliably locate and separate cells in the voxel grid system with no bias involved. By collapsing the *z*-coordinate of the neurons to the section, we limit the best spatial resolution in the *z*-axis to the section distance. As an alternative, the z coordinates of the cell bodies in a discontinuous database can be left intact and cells may be visualized in their true positions. Nevertheless, collapsing the *z*-coordinates into common planes or keeping them in their original position does not affect the density calculation as long as the voxel size is kept constant. Since the *z*-dimension of the voxels in our data analysis was equal to the section thickness and this thickness was uniform across the slices the density measures between different voxels were comparable.

Surface rendering

Since iso-density surfaces are rendered around higher density volumes, hollow spaces with lower density may be captured under the surfaces of higher density volumes. One way to uncover hollow spaces is by splicing the volumetric data with a plane and projecting the density map on that plane. Figure 5E-F is from iso-relational dataset of parvalbumin and cholinergic cells using density threshold for both cell population 5 per voxel (250×250 µm). This and other 2D maps of the density ratios indicate no signs of hollow spaces in the iso-density distributions. Another method to uncover hollow spaces is to use transparent surface rendering.

The presence of junctions between surfaces where different cell populations intersect may also complicate interpretation. When one cell population penetrates another cell population, the volume of intersection is covered by the surface of the larger volume. Ambiguities due to intersection can be resolved by showing the iso-density surfaces for individual cell types separately in different plots. The iso-relational surface map is the most complicated to interpret. It is necessary to compare it with the individual iso-density surfaces that the relation was derived from. Essentially, the iso-relational surface is rendered around the intersection between at least two cell-groups where a certain density ratio criterion is accomplished. Therefore, its shape and location must be incorporated by the iso-density surface of both cell types.

Across animal validity

In our analysis, the various cell populations from the same animal were superimposed into one common coordinate system. This was possible using the alignment algorithms in the Neurolucida system and the characteristic shape of the distribution of cholinergic cells that served as a 3D framework to incorporate the entire database (see Materials and methods). Additionally, when data were compared from different cases, we took advantage of the more versatile alignment tools of the Micro3D program (Oslo Research Park). The comparison of different brains suggests a remarkable similarity in the global and local organization of the different populations investigated in the BF. When individual renderings are combined into one scheme (for a more detailed visualization and discussion of this topics see L. Zaborszky, D.L.Buhl, S. Pobalashingham, J. Somogyi, J.G. Bjaalie, Z. Nadasdy, unpublished work) misalignments would particularly alter the configuration and location of overlapping zones between different cell pop-

ulations. The similarity of the combined renderings, however, indicates that the configuration of iso-density or iso-relational surfaces is not random.

Concluding remarks

3D reconstructions and numerical analyses, with the methods described in this paper, suggest that neurochemically defined cell populations within the entire BF, including the medial septum, diagonal band nuclei, bed nucleus of the stria terminalis, substantia innominata, and pallidal areas, are aligned in oblique-longitudinally oriented large-scale cell sheets that seem to have a specific association pattern. Within each cell system, the neurons display characteristic discontinuous distributions, including high density cell clusters. As a result of non-homogeneities within the individual cell populations and partial overlapping between different cell types, the space containing the bulk of cholinergic neurons can be considered to consist of a mosaic of various sized clusters (L. Zaborszky, D.L.Buhl, S. Pobalashingham, J. Somogyi, J.G. Bjaalie, Z. Nadasdy, unpublished work). These cholinergic cell clusters can be further specified by their dendritic orientations, input-output features and numerical relations to other neurochemically identified neurons. It is envisioned that these clusters may function as information processing units or modules in the BF and may represent special sites where functionally related cortical target areas and different input (brainstem and telencephalic) pathways are linked together. It remains to be tested in functional imaging studies in humans and multiple single unit recordings in animals whether or not the proposed structural scaffolds 'placed' into the apparently diffuse network of the BF can indeed be utilized as selective conduits in distributing prefrontal executive directives to parallel and hierarchically organized cortical processes as suggested in a recent review based upon the known BF connectional patterns, and the cognitive-neurobiological constrains of attention (Zaborszky et al. 1999).

Acknowledgement This work was supported by NIH grant 23945 to L.Z.

References

Alloway D, Crist J, Mutic, JJ, Roy SA (1999) Corticostriatal projections from rat barrel cortex has an anisotropic organization that correlates with vibrissal whisking behavior. J Neurosci 19:10908–10922

Bjaalie JG, Diggle PJ, Nikundiwe A, Karagulle T, Brodal P (1991) Spatial segregation between populations of ponto-cerebellar neurons: statistical analysis of multivariate interactions. Anat Rec 231:510–523

Bjaalie JG, Sudbo J, Brodal P (1997) Corticopontine terminal fibres form small scale clusters and large scale lamellae in the cat. Neuroreport 8:1651–1655

Braitenber V, Schutz A (1998) Cortex: statistics and geometry of neuronal connectivity. 2nd edn. Springer, Berlin Heidelberg New York

Chevalier G, Mana S (2000) Honeycomb-like structure of the intermediate layers of the rat superior colliculus, with additional observations in several other mammals: AChE patterning. J Comp Neurol 419:137–153

Csordas A, Zaborszky L (2000) A second look at the organization of the basal forebrain corticopetal system. Soc Neurosci Abstr 26: 2140

Dunnett SB, Everitt BJ, Robbins TW (1991) The basal forebrain-cortical cholinergic system: interpreting the functional consequences of excitotoxic lesions. Trends Neurosci 14: 494–501

Everitt BJ, Robbins TW (1997) Central cholinergic systems and cognition. Annu Rev Psychol 48: 649–684

Gerfen CR (1985) The neostriatal mosaic. I. Compartmental organization of projections from the striatum to the substantia nigra in the rat. J Comp Neurol 236: 454–476

Glaser JR, Glaser EM (1990) Neuron imaging with Neurolucida – a PC-based system for image combining microscopy. Comput Med Imaging Graph 14: 307–317

Graybiel AM, Ragsdale CW Jr (1978) Histochemically distinct compartments in the striatum of human, monkey, and cat demonstrated by acetylcholinesterase staining. Proc Natl Acad Sci USA 75: 5723–5726

He, S-Q, Dum RP, Strick PL (1993) Topographic organization of corticospinal projections from the frontal lobe: motor areas on the lateral surface of the hemisphere. J Neurosci 13: 952–980

Heimer L (2000) Basal forebrain in the context of schizophrenia. Brain Res Rev 31:205–235

Heimer L, Alheid GF, Zaborszky L (1985) The basal ganglia. In: Paxinos G (ed) The rat nervous system (forebrain and midbrain, vol 1). Academic Press, Sydney, pp 37–86

Heimer L, Olmos J de, Alheid GF, Zaborszky L (1991) "Perestroika" in the basal forebrain; opening the border between neurology and psychiatry. Progr Brain Res 87: 109–165

Hsu SM, Soban E (1982) Color modifications of diaminobenzidine (DAB) precipitation by metallic ions and its application for double immunohistochemistry. J Histochem Cytochem 30: 1079–1082

Jakab RL, Lernath C (1995) Septum. In: G. Paxinos (ed), The rat nervous system. 2nd edn. Academic Press, San Diego, pp 405–442

Jones BE, Muhlethaler M (1999) Cholinergic and GABAergic neurons of the basal forebrain: role in cortical activation. In: Lydic R, Baghdoyan HA (eds), Handbook of behavioral state control – cellular and molecular mechanisms. CRC Press, New York, pp 213–234

Kilgard M P, Merzenich MM (1998) Cortical map reorganization enabled by nucleus basalis activity. Science 279:1714–1718

Kiss J Z, Magloczky J, Somogyi J, Freund T F (1997) Distribution of calretinin containing neurons relative to other neurochemically identified cell types in the medial septum of the rat. Neuroscience 78:399–410

Leergaard BT, Alloway KD, Mutic JJ, Bjaalie JG (2000) Three-dimensional topography of corticopontine projections from rat barrel cortex: correlations with corticostriatal organization. J Neurosci 20:8474–8484

Malmierca MS, Leergard TB, Bajo VM, Bjaalie JG, Merchan MA (1998) Anatomic evidence of a three-dimensional mosaic pattern of tonotopic organization in the ventral complex of the lateral lemniscus in cat. J Neurosci 18:10603–10618

Mesulam M-M, (1996) The systems-level organization of cholinergic innervation in the cerebral cortex and its alterations in Alzheimer's disease. Progr Brain Res 109: 285–298

Mountcastle VB (1998) Perceptual neuroscience. The cerebral cortex. Harvard University Press, Cambridge Mass.

Paxinos G, Watson C (1998) The rat brain in stereotaxic coordinates. Academic Press, San Diego

Poobalasingham S, Pang K, Zaborszky L (1996) Distribution of neurons containing different type of calcium-binding proteins in the cholinergic basal forebrain. Soc Neurosci Abstr 22:1255

Sarter M, Bruno J P (2000) Cortical cholinergic inputs mediating arousal, attentional processing and dreaming: differential afferent regulation of the basal forebrain by telencephalic and brainstem afferents. Neuroscience 95:933–952

Szentagothai J (1978) The neuron network of the cerebral cortex: A functional interpretation. Proc R Soc Lond Biol Sci 201: 219–248

Szentagothai J (1983) The modular architectonic principle of neural centers. Rev Physiol Biochem Pharmacol 98:11–61

Vassbo K, Nicotra G, Wiberg M, Bjaalie JG (1999) Monkey somatosensory cerebrocerebellar pathways: uneven densities of corticopontine neurons in different body representations of areas 3b, 1, and 2. J Comp Neurol 406:109–128

Wainer BH, Steininger TL, Roback JD, Burke-Watson MA, Mufson EJ, Kordower J (1993) Ascending cholinergic pathways: functional organization and implications for disease models. Progr Brain Res 98:9–30

Woolf NJ (1991) Cholinergic system in mammalian brain and spinal cord. Progr Neurobiol 37:475–524

Zaborszky,L, Carlsen J, Brashear HR, Heimer L (1986) Cholinergic and GABAergic afferents to the olfactory bulb in the rat with special emphasis on the projection neurons in the nucleus of the horizontal limb of the diagonal band. J Comp Neurol 243:488–509

Zaborszky L, Pang K, Somogyi J, Nadasdy Z, Kallo I (1999) The basal forebrain corticopetal system revisited. Ann NY Acad Sci 877:339–367

Zaborszky L, Csordas A, Buhl DL, Duque A, Somogyi J, Nadasdy Z (2001) Computational anatomical analysis of the basal forebrain corticopetal system. In: Ascoli A (ed) Computational neuroanatomy: principles and methods. Humana Press, New Jersey (in press)

Zaborszky L, Buhl DL, Pobalashingham S, Somogyi J, Bjaalie JG, Nadasdy Z (2001) Distribution of 3 different calcium-binding protein-containing neurons in teh basal forebrain: A computational anatomical study. (in preparation)